Surface Force Measurements of Electrostatic and Hydrogen-Bonding Interactions between Bilayers of Glycine Amphiphiles

ARTICLE *in* LANGMUIR · APRIL 2002

Impact Factor: 4.46 · DOI: 10.1021/la011486f

6 AUTHORS, INCLUDING:

Peter Berndt
Roche
39 PUBLICATIONS **2,034** CITATIONS
SEE PROFILE

Shiv Chiruvolu
NanoGram Corporation
24 PUBLICATIONS **805** CITATIONS
SEE PROFILE

Matthew Tirrell
University of Chicago
468 PUBLICATIONS **12,617** CITATIONS
SEE PROFILE

Surface Force Measurements of Electrostatic and Hydrogen-Bonding Interactions between Bilayers of Glycine Amphiphiles

James Schneider,*,† Peter Berndt, Kraig Haverstick, Sanjay Kumar, Shiv Chiruvolu, and Matthew Tirrell*,‡

Department of Chemical Engineering and Materials Science, University of Minnesota, Minneapolis, Minnesota 55455

Received September 27, 2001. In Final Form: February 8, 2002

Using the surface-force apparatus (SFA), we have made sensitive force and adhesion measurements between Langmuir−Blodgett (LB) bilayers of a novel glycine-containing amphiphile at various pHs. The adhesion between the glycine headgroups is remarkably strong ($F/R = -80 \pm 5$ mN/m) and leads to the extraction of amphiphiles from the bilayers on surface separation. By SFA measurements and Fourier transform infrared spectroscopy on LB layers of glycine amphiphile variants, we determined that hydrogen bonding between amide and carbonyl groups on opposing surfaces is responsible for the strong adhesion. The strong adhesion is accompanied by a 7.5 Å interpenetration of the glycine headgroups. At higher pH, charging of the carboxylic acid termini gives rise to electrostatic repulsion between the surfaces and reduces the strength of adhesion. Above pH 8.0, the surface charging blocks interpenetration and the adhesion is extinguished. Analysis of the forces required for amphiphile extraction shows that these amide hydrogen bonds are much stronger than those in aqueous environments. This observation has important implications in the study of protein stability and the design of self-assembled biomaterials.

Introduction

The stability of folded proteins depends critically on the strengths of hydrogen-bonding, electrostatic, van der Waals, and hydrophobic interactions operating within them.[1] Knowledge of the relative contribution of each interaction to the overall stability of these structures would be central to the rational design of novel macromolecular assemblies[2,3] or protein-based polymers[4] with desired catalytic, binding, or structural properties. However, the complexity of folded proteins has made decoupling intermolecular force contributions challenging. Building model systems that are more amenable to quantitative study is one possible approach.

Historically, at least three key ideas have helped foster the belief that hydrophobic interactions are the dominant contributor to the stability of folded proteins. First, there is the realization that hydrogen bonds with water stabilize the *denatured* state.[5] Also, the free energy of transfer for nonpolar amino acids from water to oil is large and negative.[6] Finally, calorimetric measurements on the protein unfolding process have shown behavior similar to that for the solvation of nonpolar molecules in water.[7] Recent calorimetric measurements made on model compounds such as cyclic dipeptides,[8] asparagine-to-alanine,[9,10] and unnatural amino acid[11] mutants of well-characterized proteins indicate that hydrogen-bonding interactions make a sizable contribution to protein stability as well. An analysis of protein structural databanks concluded that in folded proteins about 68% of backbone amide groups are involved in hydrogen bonds,[12] highlighting the importance of these interactions in proteins.

Micromechanical force measurements have made possible the direct probing of intermolecular interactions in several biological systems. Using the surface-force apparatus (SFA)[13,14] and the atomic force microscope (AFM),[15] the strengths of hydrophobic,[16] electrostatic,[17] and steric[18] forces have been studied in great detail. Recently, these and other techniques have been extended to measure interactions in more complex biological systems. The streptavidin/biotin system has served as a useful model of specific ligand/receptor interactions, and their interaction forces have also been measured using the SFA[19−21]

* To whom correspondence should be addressed.

† Current address: Department of Chemical Engineering, Carnegie Mellon University, Pittsburgh, PA 15213-3890.

‡ Current address: Departments of Chemical Engineering and of Materials, University of California, Santa Barbara, CA 93106.

(1) Creighton, T. E. *Proteins*: *Structures and Molecular Properties*; W. H. Freeman: New York, 1993.
(2) Ghadiri, M. R.; Granja, J. R.; Buehler, L. K. *Nature* **1994**, *369*, 301−304.
(3) Lehn, J. M. *Science* **1993**, *260*, 1762−1763.
(4) Urry, D. W. *J. Phys. Chem. B* **1997**, *101*, 11007−11028.
(5) Kauzmann, W. *Adv. Protein Chem.* **1959**, *14*, 1−63.
(6) Nozaki, Y.; Tanford, C. *J. Biol. Chem.* **1971**, *246*, 2211−2217.
(7) Privalov, P. L.; Gill, S. J. *Adv. Protein Chem.* **1988**, *39*, 191−234.
(8) Murphy, K. P.; Gill, S. J. *J. Mol. Biol.* **1991**, *222*, 699−709.
(9) Pace, C. N. *Methods Enzymol.* **1995**, *259*, 538−554.
(10) Pace, C. N.; Shirley, B. A.; McNutt, M.; Gajiwala, K. *FASEB J.* **1996**, *10*, 75−83.
(11) Koh, J. T.; Cornish, V. W.; Schultz, P. G. *Biochemistry* **1997**, *36*, 11314−11322.
(12) Stickle, D. F.; Presta, L. G.; Dill, K. A.; Rose, G. D. *J. Mol. Biol.* **1992**, *226*, 1143−1159.
(13) Leckband, D. *Nature* **1995**, *376*, 617−618.
(14) Tirrell, M. *Curr. Opin. Colloid Interface Sci.* **1997**, *2*, 70−75.
(15) Colton, R. J.; Barger, W. R.; Baselt, D. R.; Corcoran, S. G.; Koleske, D. D.; Lee, G. U. *Atomic Force Microscopy*: *Surface Forces, Adhesion and Nanomechanics Measurements*; van Ooij, W. J., Anderson, H. R., Eds.; VSP: Amsterdam, 1998; pp 1−27.
(16) Christenson, H. K. *The Long-Range Attraction between Macroscopic Hydrophobic Surfaces*; Schrader, M. E., Loeb, G., Eds.; Plenum Press: New York, 1992; pp 29−51.
(17) Israelachvili, J.; Adams, G. E. *J. Chem. Soc., Faraday Trans. 1* **1978**, *74*, 975−1001.
(18) Patel, S. S.; Tirrell, M. *Annu. Rev. Phys. Chem.* **1989**, *40*, 597−635.
(19) Helm, C. A.; Knoll, W.; Israelachvili, J. N. *Proc. Natl. Acad. Sci. U.S.A.* **1991**, *88*, 8169−8173.
(20) Leckband, D. E.; Israelachvili, J. N.; Schmitt, F.-J.; Knoll, W. *Science* **1992**, *255*, 1419−1421.

10.1021/la011486f CCC: $22.00
Published on Web 04/17/2002

and AFM.[22−24] These techniques have also been used to probe interactions between complementary DNA base pairs.[25−28]

Here, we make micromechanical force measurements between glycine-functionalized amphiphiles as a model of hydrogen-bonding interactions in proteins. Organized layers of glycine can be prepared by Langmuir−Blodgett (LB) deposition[29,30] once the glycine molecule is covalently linked to an amphiphilic tail. A flexible synthetic technique has been developed[31] by which activated amphiphilic molecules are synthesized and coupled to glycine using peptide chemistry, affording precise control of the chemistry of the tail and headgroup. This study extends preliminary force measurements[32] made on the $(C_{16})_2$−Glu−C_2−Gly variant (Figure 1), possessing two 16-carbon tails ($(C_{16})_2$), a glutamic acid tail linker (Glu), a 2-carbon spacer (C_2), and glycine (Gly). The N-terminus of glycine is covalently linked to the amphiphile, and the carboxylic acid of the C-terminus is distal to the tails.

A reliable protocol has been established to measure micronewton forces between LB layers using the SFA.[21,32,33] Briefly, the SFA makes micronewton force measurements between atomically smooth mica substrates at molecular separations. Forces are ascertained by the deflection of supporting springs, and distances are resolved with angstrom resolution by an optical interferometry method.[34] The interaction geometry is well-defined, allowing for facile comparison of experimental data to theoretical models. The interferometry technique makes absolute measurements of parameters vital for molecular force and adhesion studies, including surface separation distance, adhesive contact area, and local surface curvature. The direct transfer of monolayer films in the LB process ensures that the film has the appropriate composition and thickness and also serves as a useful diagnostic tool.

Choosing to anchor the glycine molecules to solid supports by lipidation and LB deposition places the interacting glycine molecules near the hydrophobic environment of the lipid membrane, mimicking the environment in and around the molten globule of hydrophobic residues inside folded proteins. Similarly, the hydrophobic interactions that help stabilize the molten globule also help stabilize these LB layers. The interesting competition between hydrophobic and hydrogen-bonding interactions we present here should be relevant to intramolecular competitions when the folded protein is subjected to thermal, chemical, or mechanical denaturation processes.

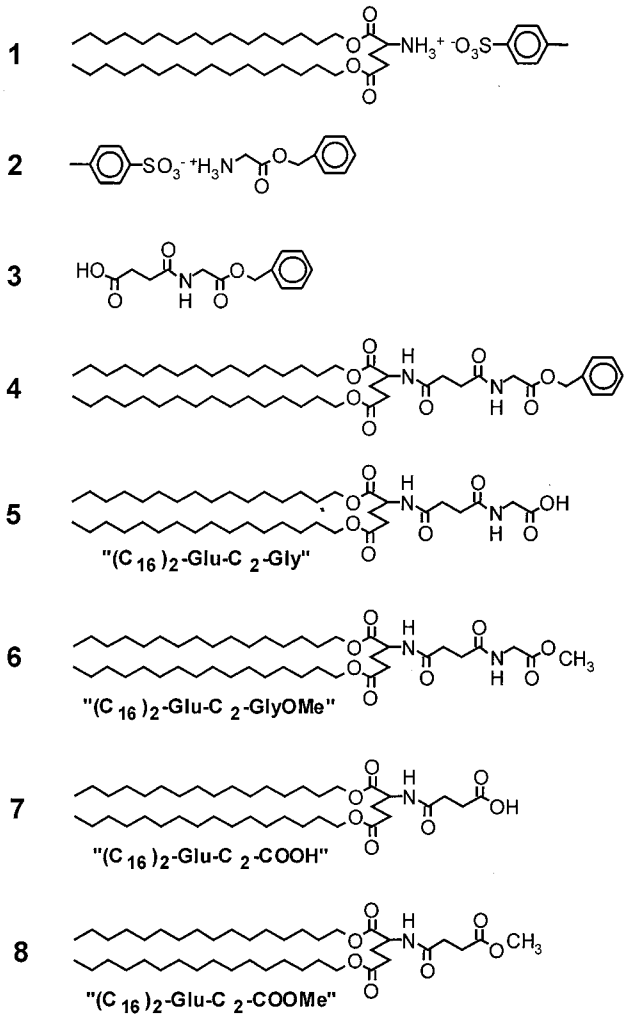

Figure 1. Molecular structure of synthesis intermediates (**1**−**4**) and functional variants of the glycine amphiphile (**5**−**8**).

Experimental Methods

In the descriptions that follow, all solvents are HPLC grade, and all reagents are ACS grade. "Water" is deionized water purified in a Milli-Q UV Plus unit (Millipore) to a final resistivity of 18.2 MΩ cm. Glassware was cleaned using a 1:1 chloroform/methanol solution or chromate cleaning solution as necessary.

Synthesis of Glycine Amphiphiles. The glycine amphiphiles were synthesized by a multistep solution procedure. Intermediates in this synthesis are depicted in Figure 1. Briefly, amphiphile tail groups were synthesized by a carboxylic acid−alcohol condensation reaction yielding **1**. Separately, Boc-protected glycine salt **2** was linked to a succinic anhydride spacer to form **3**. **1** and **3** were coupled by carbodiimide chemistry to form **4**, which was subsequently deprotected by catalytic hydrogenation to yield the glycine amphiphile **5**. **6** (the methyl ester of **5**) was created using the above procedures, but using the chloride salt of reagent **2** and a version of **3** without the terminal phenyl group, since no protection of the terminus was required. **7** was created by linking the succinic anhydride spacer directly to **1**, using the same chemistry as the glycine-spacer linkage reaction. **8** (the methyl ester of **7**) was created similarly, but using the monomethyl ester of succinic acid in place of succinic anhydride. Tail-length variants of **5**−**8** were created using longer- or shorter-chain alcohols in the tail-linking reaction as needed. Additional synthesis and characterization details are available.[31]

Systematic Naming Scheme. We will refer to **5**−**8** and their tail-length variants hereafter using a systematic naming scheme (Figure 1) based on chemical structure. For example, **5** is called $(C_{16})_2$−Glu−C_2−Gly, where (C_{16}) refers to the two 16-carbon tails, Glu refers to the L-glutamic acid linker, C_2 refers to the two-methylene spacer added by succinylation, and Gly refers to the

(21) Leckband, D.; Müller, W.; Schmitt, F.-J.; Ringsdorf, H. *Biophys. J.* **1995**, *69*, 1162−1169.
(22) Lee, G. U.; Kidwell, D. A.; Colton, R. J. *Langmuir* **1994**, *10*, 354−357.
(23) Moy, V. T.; Florin, E. L.; Gaub, H. E. *Colloids Surf., A* **1994**, *93*, 343−348.
(24) Moy, V. T.; Florin, E. L.; Gaub, H. E. *Science* **1994**, *266*, 257−259.
(25) Berndt, P.; Kurihara, K.; Kunitake, T. *Langmuir* **1995**, *11*, 3083−3091.
(26) Kurihara, K.; Abe, T.; Nakashima, N. *Langmuir* **1996**, *12*, 4053−4056.
(27) Boland, T.; Ratner, B. D. *Proc. Natl. Acad. Sci. U.S.A.* **1995**, *92*, 5297−5301.
(28) Lee, G. U.; Chrisey, L. A.; Colton, R. J. *Science* **1994**, *266*, 771−773.
(29) Ulman, A. *An Introduction to Ultrathin Organic Films*; Academic Press: New York, 1991.
(30) Zasadzinski, J. A.; Viswanathan, R.; Madsen, L.; Garnaes, J.; Schwartz, D. K. *Science* **1994**, *263*, 1726−1733.
(31) Berndt, P.; Fields, G.; Tirrell, M. *J. Am. Chem. Soc.* **1995**, *117*, 9515−9522.
(32) Schneider, J.; Berndt, P.; Haverstick, K.; Kumar, S.; Chiruvolu, S.; Tirrell, M. *J. Am. Chem. Soc.* **1998**, *120*, 3508−3509.
(33) Marra, J.; Israelachvili, J. *Biochemistry* **1985**, *24*, 4608−4618.
(34) Israelachvili, J. N. *J. Colloid Interface Sci.* **1972**, *44*, 259−272.

glycine terminus. GlyOMe refers to the methyl ester of glycine. For the glycine-free variants, COOH refers to the carboxylic acid terminus left after succinylation. COOMe is its methyl ester.

Pressure−Area Isotherms. Pressure−area isotherms and LB depositions were carried out using a computer-controlled, liquid-cooled KSV 5000 Langmuir trough in a dust-free laminar flow hood. Surface pressure measurements were made using a platinum Wilhelmy plate. The movement of the barrier was controlled by a computer algorithm that continually decreased the speed of the barrier movement down to 3 mm/min in response to the increase in surface pressure.

LB Technique. For AFM studies, thin mica disks (diameter of 2.5 cm^2) were held on edge by clean stainless steel tweezers hung onto the dipper. For SFA studies, mica-covered silica lenses were held from the side by clean stainless steel grippers. For the DPPE/$(C_{16})_2$−Glu−C_2−Gly bilayers, the DPPE monolayer was compressed to a deposition pressure (π_{dep}) of 41 mN/m and this surface pressure was maintained for 5 min to equilibrate the film. The mica was then slowly (1 mm/min) lifted through the film, depositing a monolayer of DPPE. The mica was allowed to dry for 15 min before a monolayer of glycine amphiphile was spread and compressed to $\pi_{dep} = 35$ mN/m. After equilibration, the mica substrates were slowly (1 mm/min) lowered through the film until completely submerged. Transfer ratios (measured on large mica sheets, R_t) were 1.00 ± 0.05 for both deposition processes. For Fourier transform infrared (FTIR) spectroscopy, CaF_2 plates were rinsed thoroughly in chloroform/methanol solution prior to LB deposition for cleaning. Over subphases of appropriate pH, four monolayers of $(C_{16})_2$−Glu−C_2−Gly at π_{dep} = 41 mN/m were transferred first on the downstroke ($R_t = 0.5 \pm 0.1$), then on the upstroke ($R_t = 0.8 \pm 0.1$), and so forth.

FTIR Spectroscopy. CaF_2 plates were stored in an evacuated desiccator overnight before installation in the IR spectrometer (Nicolet Magna 550). After purging the sample area with dry nitrogen for at least an hour, FTIR spectra were taken in transmission mode, and the data were analyzed using Omnic 1.2a software (Nicolet Instruments). Background spectra of the uncoated plate were subtracted from the final spectra. Spectra were baseline-corrected as necessary.

Atomic Force Microscopy. AFM measurements on LB bilayers were carried out by a Digital Instruments Nanoscope II unit, using AFM probes from Digital Instruments. After LB deposition, the submerged mica disks were transferred underwater (using shallow beakers) to a clean plastic container filled with Milli-Q-purified water and carried to the AFM facility. A Teflon-coated Viton O-ring (Precision Associates, Minneapolis, MN) was rinsed in methanol, dried, and placed directly onto the submerged mica substrate. The mica disk with the O-ring was placed on the AFM piezoelectric stage, and the fluid cell containing the AFM tip was precisely lowered onto the O-ring. AFM measurements were made using a software package provided by Digital Instruments.

Surface-Force Apparatus. SFA measurements were carried out using a stainless steel Mark II SFA built at the University of Minnesota, using a double-cantilever leaf spring of spring constant 3.3×10^5 dyn/cm and cylindrically curved silica lenses (radius of curvature (R) = 2 cm). A differential spring mechanism was used to translate the leaf spring and its lens with nanometer precision. Images of the FECO (fringes of equal chromatic order) interference fringes were obtained using a liquid-cooled CCD camera (Photometrics).

Following the protocol of Israelachvili,[17] 1−3 μm sheets of ruby mica (Mica New York) were cleaved from a thick mica slab in a laminar flow hood. Coupons which did not give rise spontaneously to intimate van der Waals contact with the backing sheet were rejected. A 450 Å thick layer of silver was thermally evaporated onto the backing sheet at a deposition rate of 1 Å/s. Mica coupons were glued onto lenses as previously described using EPON 1004 epoxy resin (Shell). The SFA was placed in its optical setup for a mica thickness measurement in air. After the LB layers were deposited onto the mica-covered lenses, the SFA was placed on its side and rinsed several times with water and refilled. Using glass beakers, the lenses were transferred to and mounted in the SFA, keeping the mica submerged at all times. The SFA was then moved to a thermostated cabinet (T = 25−30 °C) and left for 2−8 h to reach thermal equilibrium. The location of the micrometer and the position of the FECO in the spectrometer were recorded at 25 Å intervals in mica/mica separation distance, allowing 10 s for the spring mechanism to stabilize, until contact was established as perceived by a flattening of the FECO. Pull-off forces were measured by calculating the surface separation after jump-out, which is roughly equal to the spring deflection just prior to jump-out. Radii of curvature were measured by analysis of the FECO images. A dove prism was used to rotate images and measure the radius in orthogonal sections. The radius was taken to be the geometric mean of these values.

The pH of the SFA subphase was changed by injecting a few milliliters of concentrated, unbuffered HNO_3 or KOH (high purity, Aldrich) as needed using a clean glass syringe. The surfaces were moved together and apart several times to mix the solution, and measurements were made after about 8 h mixing time. Citrate/phosphate buffer is a 0.4 mM solution of citric acid and monobasic potassium phosphate (Aldrich, high purity), with pH adjusted using the above titrants. All force data presented here have distance axes with "zero" corresponding to bare-mica/bare-mica contact, as measured during the initial thickness measurement.

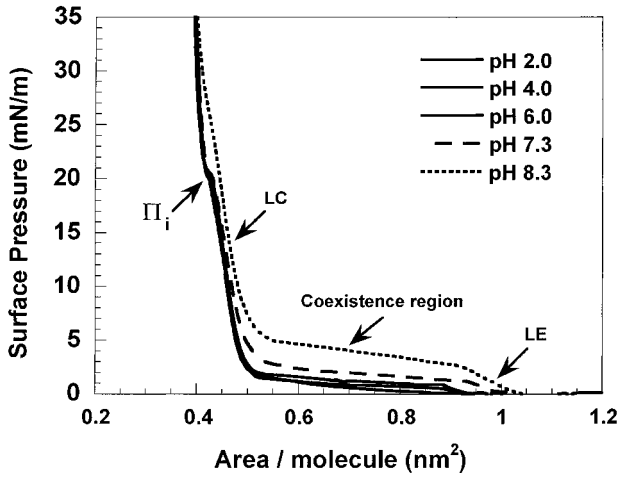

Figure 2. Pressure−area isotherms for $(C_{16})_2$−Glu−C_2−Gly at various pHs and 1 mM KBr. Note the inflection observed at Π_i.

Results

Monolayer Properties. Most of the work presented here was performed using the $(C_{16})_2$−Glu−C_2−Gly glycine amphiphile. Its Langmuir isotherm (Figure 2) has a pH-dependent phase behavior, with a pronounced liquid-expanded region, a liquid-condensed region, and an apparent two-phase coexistence region between them. The high collapse pressure (π_C = 55 mN/m) attests to the purity and stability of the monolayer. Below pH 8, an inflection in the isotherm is observed just before the phase transition (π_i), which we ascribe to a conformational change in the sizable headgroup of $(C_{16})_2$−Glu−C_2−Gly. As the pH is increased from 6.0 to 8.3, the monolayer is destabilized as indicated by a shift of the phase-transition region to progressively higher surface pressures.

The methyl ester derivative of $(C_{16})_2$−Glu−C_2−Gly, $(C_{16})_2$−Glu−C_2−GlyOMe, has a similar pressure−area isotherm (Figure 3), but the inflection is significantly more pronounced, likely due to additional packing frustration introduced by the terminal methyl group. Isotherms of $(C_{16})_2$−Glu−C_2−GlyOMe were not significantly affected by pH changes over a wide range (pH 4−9), indicating that all charging of $(C_{16})_2$−Glu−C_2−Gly is due to the deprotonation of the terminal carboxylic acid in the pH range 6−8. Because the monolayer is destabilized by the addition of this methyl group, any attempt to LB transfer $(C_{16})_2$−Glu−C_2−GlyOMe causes the layer to collapse. Extending each tail by two methylene groups confers added stability to the layer so that $(C_{18})_2$−Glu−C_2−

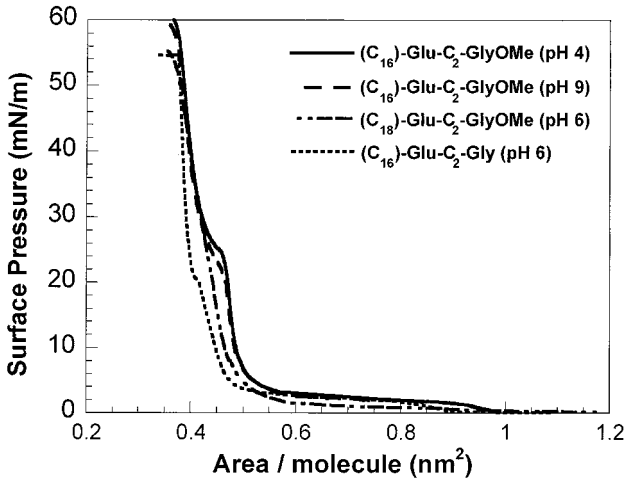

Figure 3. Pressure−area isotherms for methyl ester derivatives of glycine amphiphiles. The inflection is more pronounced for these molecules, and more pressure is required to pack the amphiphile tails closely. There are no significant changes in the isotherms of $(C_{18})_2$−Glu−C_2−GlyOMe over a wide pH range.

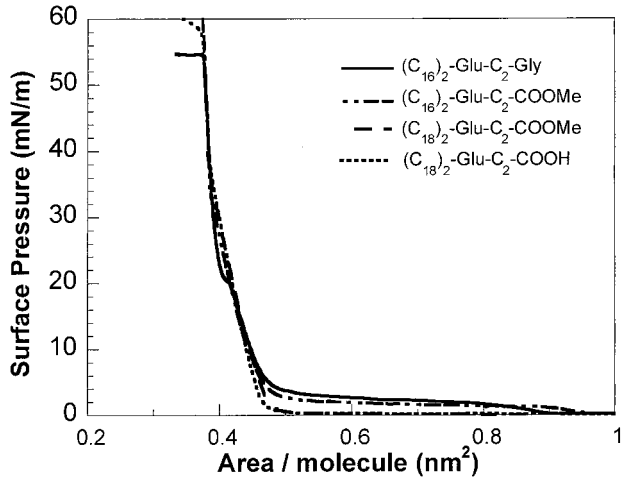

Figure 4. Pressure−area isotherms for glycine-free variants of $(C_{16})_2$−Glu−C_2−Gly in pure water (pH 5.6). No inflection is observed in the isotherms for these variants.

GlyOMe transfers nicely (transfer ratio, $R_t = 1.00 \pm 0.05$) onto hydrophobized mica.

Pressure−area isotherms of glycine-free variants of $(C_{16})_2$−Glu−C_2−Gly (Figure 4) also lack the inflection observed for $(C_{16})_2$−Glu−C_2−Gly. $(C_{16})_2$−Glu−C_2−COOH and $(C_{16})_2$−Glu−C_2−COOMe give stable isotherms with high collapse pressures but also collapse during LB deposition. Again, adding two methylene units to each tail helps stabilize the monolayer as judged by the lowering of the surface pressure in the coexistence region. $(C_{18})_2$−Glu−C_2−COOH transfers readily onto hydrophobized mica ($R_t = 1.00 \pm 0.05$).

FTIR Spectroscopy. FTIR spectra of $(C_{16})_2$−Glu−C_2−Gly bilayers were obtained by depositing these layers at various pHs and drying the bilayers for several hours for measurement in the dry state. These spectra confirm that charging of the carboxylic acid termini of the $(C_{16})_2$−Glu−C_2−Gly occurs as the deposition pH is increased from 5.6 to 8.5. Significant peaks and vibrational assignments[35] based on FTIR spectra of small molecules are listed in Table 1. Bilayers deposited at pH 5.6 have a single dominant carbonyl peak located at 1739 cm^{-1}. FTIR spectra for bilayers deposited at pH 8.5 have two additional peaks corresponding to carbonyl stretches in carboxylate groups (1592 and 1406 cm^{-1}), and the acid carbonyl stretch is attenuated (1739 cm^{-1}).

Table 1. Vibrational Assignments[a] for FTIR Spectra of $(C_{16})_2$−Glu−C_2−Gly LB Layers

vibrational assignment	wavenumber (cm^{-1}) pH 5.6	pH 8.5
amide A stretch	3310.2	3311.8
$-CH_3$ asymmetric stretch	2955.6	2955.6
$-CH_2-$ asymmetric stretch	2916.5	2917.5
$-CH_2-$ symmetric stretch	2850.2	2850.3
C=O symmetric stretch (carboxylic acid + ester)	1735.6	1739.1
amide I stretch	1642.5	1652.4
C=O symmetric stretch (carboxylate)		1592.0
amide II stretch	1536.5	1518.9
$-CH_2-$ scissors	1468.9	1467.8
C=O asymmetric stretch (carboxylate)		1406.1

[a] References 35−37.

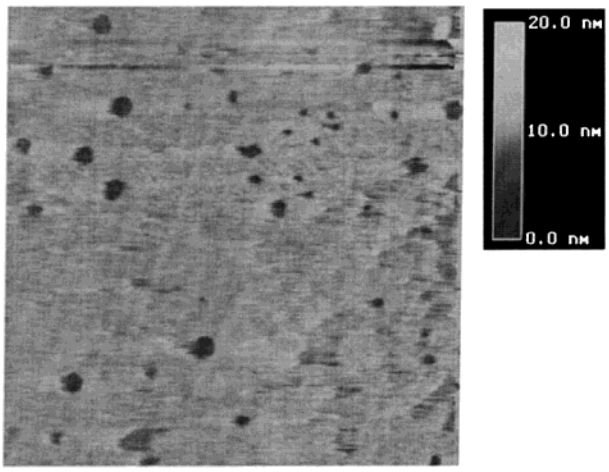

Figure 5. Contact-mode AFM image of a $(C_{16})_2$−Glu−C_2−Gly monolayer deposited onto hydrophobized mica at $\pi_{dep} = 35$ mN/m (pure water). The image size is 5 μm × 5 μm. Pinhole defects have a depth of about 30 Å.

FTIR spectra (Table 1) also demonstrate that a high degree of hydrogen bonding occurs between the glycine headgroups at low pH. At pH 5.6, the amide A peak (3310 cm^{-1}) and the amide I peak (3310 cm^{-1}) have wavenumbers significantly lower than expected for amide groups not involved in hydrogen bonding (3450[35] and 1666 cm^{-1},[36] respectively). The carbonyl symmetric stretch peak at 1736 cm^{-1} represents contributions from those in the tail-linker region and the terminal carboxylic acid. As a result, it cannot be determined if the peak is significantly shifted from its non-hydrogen-bonded location (1800−1740 cm^{-1}).[37] At pH 8.2, the amide I peak (1652 cm^{-1}) is located closer to its non-hydrogen-bonded location (1666 cm^{-1}) than it is at pH 5.6 (1643 cm^{-1}). This indicates an attenuation of glycine−glycine hydrogen bonding with increasing pH.

Surface-Force Measurements. Force measurements were made on LB monolayers of glycine amphiphile deposited onto mica which was first hydrophobized by LB deposition of a monolayer of DPPE. A contact-mode AFM image (Figure 5) of the submerged composite DPPE/$(C_{16})_2$−Glu−C_2−Gly LB bilayer on mica shows a few pinhole defects, similar to those observed for LB-deposited lipid

(35) Szymanski, H. A. *A Systematic Approach to the Interpretation of Infrared Spectra*; Hertillon Press: Buffalo, 1967.

(36) Jackson, M.; Mantsch, H. H. *Crit. Rev. Biochem. Mol. Biol.* **1995**, *30*, 95−120.

(37) Socrates, G. *Infrared Characteristic Group Frequencies*; John Wiley & Sons: New York, 1994.

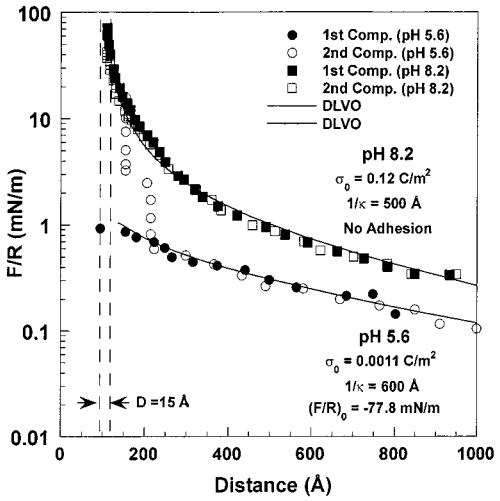

Figure 6. SFA force profiles for $(C_{16})_2-Glu-C_2-Gly$ monolayers in pure water at pH 5.6 and 8.2. D_0 is 15 Å smaller at pH 5.6 than at pH 8.2. At pH 5.6, a large adhesion is measured, leading to the bilayer disruption observed on second compression. No adhesion or bilayer disruption is observed at pH 8.2. The contact bilayer thickness (D_0) was 15 Å smaller in the adhesive case (pH 5.6), suggesting that headgroup interpenetration is occurring on contact. OHP for the pH 5.6 DLVO fit was shifted accordingly (see text).

bilayers.[38] The defects are about 3 nm deep and 0.1−0.3 μm in diameter. While we certainly would expect these pinholes to impact the SFA data when present in the contact zone, they are fairly far apart and observable by the FECO fringes (all data presented here had smoothly varying FECO). AFM images were stable to repeated contact scanning.

SFA force curves for identical $(C_{16})_2-Glu-C_2-Gly$ monolayers in pure water (pH 5.6) are shown in Figure 6. On first approach, an exponentially increasing repulsion is observed beginning at $D = 1000$ Å, eventually rising to $F/R = 1$ mN/m. The repulsion is well described by a Derjaguin−Landau−Verwey−Overbeek (DLVO) fit, which accounts for electrostatic double-layer interactions by a solution of the Poisson−Boltzmann (PB) equation[39] and van der Waals interactions between the surfaces using a Hamaker constant (A_H) expression based on SFA measurements on LB bilayers of dipalmitoylphosphatidylcholine (DPPC) bilayers in water ($A_H = 7 \times 10^{-21}$ J).[33] We found our fits to be fairly insensitive to the choice of A_H, and we avoided more involved treatments, such as the consideration of retardation effects. The PB equation was solved by a Newton−Raphson method, varying the surface charge density (σ_0) and the Debye screening length ($1/\kappa$) until a satisfactory fit to the data was achieved. The constant charge boundary condition gave the best fits.

To make satisfactory DLVO fits, it was necessary to shift the outer Helmholtz plane (OHP) to account for the interpenetration of glycine headgroups on contact; in this case, the separation distance (D) was shifted 15 Å from the contact bilayer thickness (D_0) (Figure 7). As such, the nominal bilayer thickness (l_m) is 7.5 Å larger than half of the in-contact bilayer thickness. Correcting for the thickness shift, the fits of first approach data for these bilayers at pH 5.6 had $1/\kappa = 600$ Å and $\sigma_0 = 0.0090$ C/m^2. Given the density of $(C_{16})_2-Glu-C_2-Gly$ deposited (molecular area, $a_{dep} = 40$ Å^2), the fraction of headgroups charged (f) is related to σ_0:

$$f = \frac{\sigma_0 a_{dep}}{e} \qquad (1)$$

where e is the elementary charge. Using (1), the fit to the pH 5.6 data in Figure 7 has the bilayers 1.8% charged and the equivalent charge screening of a 2.6×10^{-5} M solution of 1:1 electrolyte.

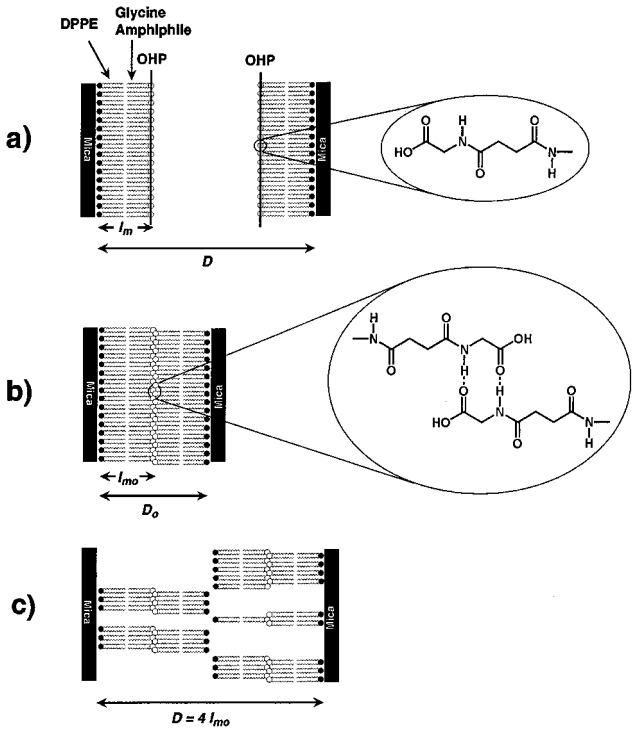

Figure 7. Definition of bilayer thickness parameters (a) and proposed molecular mechanism for the strong adhesion and failure of the composite DPPE/$(C_{16})_2-Glu-C_2-Gly$ bilayers. While in contact (b), the headgroups interpenetrate slightly and form interlayer hydrogen bonds which are maintained on separation (c), leading to the disruption of the bilayers. D refers to the separation distance between the mica surfaces, and l_m is the distance between the mica surface and the OHP, nominally the bilayer thickness. The in-contact values are assigned a subscript zero.

After overcoming the electrostatic repulsion ($F/R = 1$ mN/m), the surfaces jump into contact at $D_0 = 95$ Å (Figure 6). Since two composite bilayers are trapped between the mica sheets at this point (including the hydrophobizing DPPE), we infer that l_{m0} is about 48 Å. Space-filling calculations show the fully extended length of a DPPE molecule to be 26 Å,[33] and similar calculations for the $(C_{16})_2-Glu-C_2-Gly$ molecule, considering the lengths of amino acids in fully extended peptides,[1] have its length as 28 Å. The sum of the two (54 Å) compares favorably with the measured l_{m0}, but subtle changes in the alignment of the SFA optics following the removal of the mica substrates for LB deposition adds an uncertainty in D of about 10 Å.

While in contact, the FECO interference fringes of the SFA have a flat feature whose size is related to the adhesive contact area. As the surfaces were unloaded, a sharp discontinuity in the smooth profile of the FECO is observed at the edge of the flat feature, a shape predicted by the Johnson−Kendall−Roberts (JKR) adhesion theory under strongly adhesive conditions.[40] The FECO would appear smoothly rounded throughout the measurement

(38) Hui, S. W.; Viswanathan, R.; Zasadzinski, J. A.; Israelachvili, J. N. *Biophys. J.* **1995**, *68*, 171−178.
(39) Chan, D. Y. C.; Pashley, R. M.; White, L. R. *J. Colloid Interface Sci.* **1980**, *77*, 283−285.

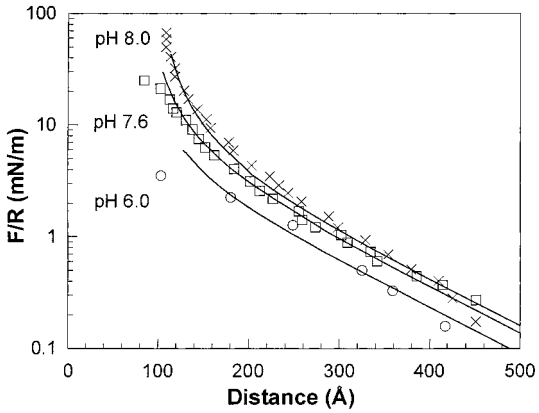

Figure 8. SFA force profiles for $(C_{16})_2$−Glu−C_2−Gly monolayers in 1 mM KBr at pH 6.0, 7.6, and 8.0, demonstrating a steadily increasing electrostatic repulsion with increasing pH. OHP for the DLVO fits is set at $D = D_0 + 15$ Å in each case (see text).

Table 2. Summary of Pull-Off Force Data for $(C_{16})_2$−Glu−C_2−Gly Monolayers in Pure Water (pH 5.6)

$-P_0$ (dyn)	R (cm)	$-(F/R)_0$ (mN/m)	D_0 (Å)
143	1.57	90.9	97
129	1.59	81.1	108
173	2.51	68.8	124
173	2.22	77.8	120
224	2.51	89.1	107
228	2.59	88.1	124
	mean	80 ± 5	113 ± 10

cycles in the absence of strong adhesion. A large pull-off force ($-(F/R)_0 = 78 \pm 5$ mN/m) was required to separate the surfaces after initial contact, and this value was confirmed by repeated measurements (Table 2). F/R was 80 ± 5 mN/m, and D_0 averaged 113 Å, giving $l_m = 57$ Å. DLVO fits using $\sigma_0 = 0.0011$ C/m^2 described all force profiles well, but the Debye length varied slightly owing to small differences in the ionic strength of the pure water from run to run.

The force profile measured on second approach at pH 5.6 is about the same as that for first approach until $D = 240$ Å, where steep repulsive barriers are observed. The surfaces cannot be brought any closer together than $D = 180$ Å without damaging the mica (as judged by the rough appearance of the FECO). A small pull-off force is required to separate the surfaces in this case ($-(F/R)_0 = 9.4 \pm 1.0$ mN/m). Because the barriers are about one and two bilayer thicknesses apart, we believe they represent steric interactions between surfaces disrupted as amphiphiles are extracted from the bilayers to maintain contact between the glycine headgroups as shown in Figure 7. Similar amphiphile extraction has been reported between biotinylated monolayers bridged by streptavidin[19] and carboxylic acid terminated monolayers bridged by calcium ions.[41]

Force measurements were made on these bilayers in the pH range 6.0−8.0, using a controlled ionic strength (1 mM KBr) to avoid pK_a shifts owing to double-layer effects. SFA force curves for $(C_{16})_2$−Glu−C_2−Gly monolayers show a gradual increase in electrostatic repulsion and a gradual decrease in pull-off force with increasing pH (Figure 8, Table 3). All measurements under adhesive conditions showed the bilayer disruption on second approach and were DLVO-fitted with the OHP placed at $D = D_0 + 15$ Å. The continual decrease in pull-off force with increasing pH is due in part to the greater long-range electrostatic barrier that must be overcome before reaching the adhesive minimum of the interaction potential. To isolate the contribution from short-range attractive forces, it is useful to define the attractive part of the pull-off force ($(F/R)_{0,at}$) obtained by adding the repulsive force experienced just prior to jump-in,[42] which in our case was the maximum repulsive force $(F/R)_{max}$:

$$-\left(\frac{F}{R}\right)_{0,at} = -\left(\frac{F}{R}\right)_0 + \frac{F}{R}\Big|_{max} \qquad (2)$$

Figure 9 is a summary of these intermediate pH data, demonstrating a coincidence between the increase in charging with a decrease in the attractive part of the pull-off force. The blocking of short-ranged attractive interactions has about the same critical pH range as the charging process, which suggests that these two processes are related.

At pH 8.0, the magnitude of the electrostatic repulsion increased dramatically due to the deprotonation of surface carboxylic acid groups. The DLVO-fitted σ_0 corresponds to 30% charging of the layers under these conditions. The adhesion between the surfaces was completely extinguished as well, with no perceivable pull-off force. Furthermore, the FECO fringes exhibited no discontinuity near the contact area, as predicted by the Hertz theory, which described the deformation of contacted elastic bodies with no mutual adhesion.[40] Subsequent force profiles gave identical force curves, with no evidence of bilayer damage, even after several contacts. Force curves measured on expansion were indistinguishable from those measured on compression.

When measured on neighboring spots to preserve the optical alignment, D_0 was found to be about 15 Å larger under the nonadhesive pH 8.5 conditions, confirming the headgroup interpenetration model. Since alkyl tails are very closely packed in these monolayers, the rearrangement is likely taken up by the headgroups, as in a mutual interpenetration. These rearrangements expose additional hydrogen-bonding amine groups to the interface.

Taking advantage of our flexible synthetic technique, we can make small functional changes in the $(C_{16})_2$−Glu−C_2−Gly molecule to better pinpoint the precise functional groups involved in the strong adhesion. SFA force data between $(C_{18})_2$−Glu−C_2−GlyOMe monolayers (Figure 10) were nearly identical to those for $(C_{16})_2$−Glu−C_2−Gly monolayers in pure water (pH 5.6). A long-range electrostatic repulsion was observed beginning at $D = 1000$ Å, and the bilayers jumped into a strong adhesive contact at about $F/R = 0.4$ mN/m. The fitted surface charge density was extremely small (0.00062 C/m^2) and is likely brought about by trace byproducts of the amphiphile synthesis or adsorbed ions. A comparably large pull-off force ($(-(F/R)_0 = 75 \pm 5$ mN/m) was required to separate the surfaces. On second compression, the steep steric barriers characteristic of amphiphile pull-off were also observed. The remarkable similarity of these data to those for the uncharged $(C_{16})_2$−Glu−C_2−Gly monolayers rules out the possibility that interfacial carboxylic acid dimers alone can link the two bilayers when in contact.

SFA force data measured between $(C_{18})_2$−Glu−C_2−COOH monolayers (Figure 11) showed similar force behavior but dramatically different adhesive behavior.

(40) Horn, R. G.; Israelachvili, J. N.; Pribac, F. *J. Colloid Interface Sci.* **1987**, *115*, 480−492.

(41) Claesson, P. M.; Berg, J. M. *Thin Solid Films* **1989**, *176*, 157−164.

(42) Leckband, D. E.; Helm, C. A.; Israelachvili, J. *Biochemistry* **1993**, *32*, 1127−1140.

Table 3. Summary of Force and Adhesion Data for the Interaction of $(C_{16})_2$−Glu−C_2−Gly Monolayers at Various pHs and Ionic Strengths

pH	σ_0 (C/m^2)	$1/\kappa$ (Å)	fraction charged (f)	$-(F/R)_0$ (mN/m)	$-(F/R)_{0,at}$ (mN/m)	W_a (mJ/m^2)	fraction bonded	fraction bonded/ unchg pair
5.6	0.0011	600	0.0028	80 ± 5	80	17	0.11	0.11 ± 0.01
6.0	0.0090	100	0.023	74 ± 5	76	16	0.11	0.11 ± 0.01
6.8	0.015	150	0.038	54 ± 5	62	13	0.09	0.10 ± 0.01
7.6	0.054	100	0.14	38 ± 4	55	12	0.08	0.11 ±0.01
8.0	0.12	100	0.30	0	0	0	0	0
8.2	0.12	500	0.30	0	0	0	0	0

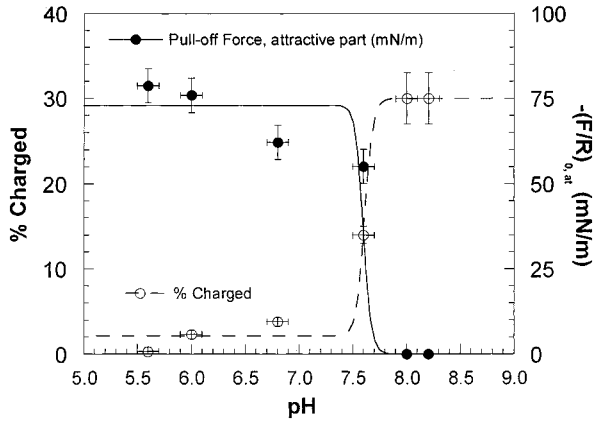

Figure 9. Adhesive titration curve summarizing pull-off force (attractive part) and extent of charging data in pure water (pH 5.6) and 1 mM KBr (others). Sigmoidal fits are presented to guide the eye and are centered near pH 7.6.

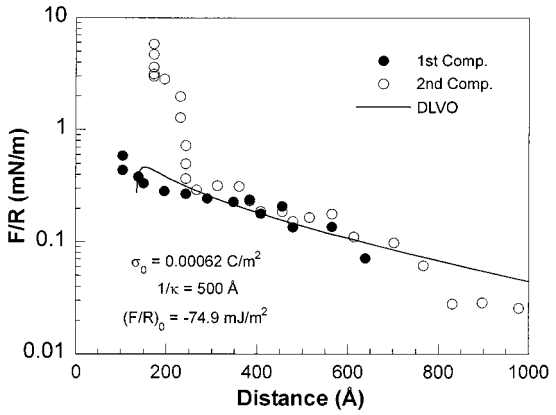

Figure 10. SFA force profiles for $(C_{16})_2$−Glu−C_2−GlyOMe monolayers in pure water (pH 5.6). The force and adhesion data are very similar to those for the uncharged $(C_{16})_2$−Glu−C_2−Gly monolayers (Figure 5). OHP for the DLVO fits is set at D_0 + 15 Å to account for interpenetration.

At pH 8.3, a large electrostatic repulsion is observed with no adhesion, but after lowering the pH to 5.4, only a small pull-off force was measured between the monolayers ($-(F/R)_0$ = 11 ± 3 mN/m). The electrostatic repulsion was attenuated, and D_0 was 15 Å lower than that at pH 8.3, signaling interpenetration. Even though the headgroup rearrangements and low surface charge were present here, the strong adhesion was not. It appears that the surface-accessible amine group of the glycine amphiphile is necessary to achieve it.

Discussion

The main observation here is a remarkably strong adhesion between LB layers of glycine amphiphiles that is attenuated by the pH-induced charging of their carboxylic acid termini. Because the amphiphiles are extracted during surface separation, the strong adhesion is

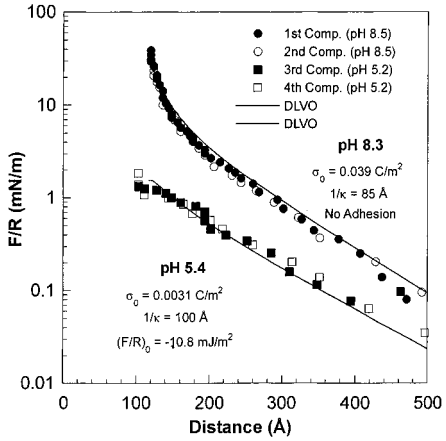

Figure 11. SFA force profiles for $(C_{18})_2$−Glu−C_2−COOH monolayers in 1 mM KBr, measured at the same spot (first at pH 8.3 and then at pH 5.4). For both fits, the OHP for DLVO fits was set to $D = D_0$ value measured at pH 8.3. Unlike the $(C_{16})_2$−Glu−C_2−Gly case (Figure 5), only a small pull-off force is observed at low pH.

not a direct measure of headgroup−headgroup interactions, such as hydrogen bonding. However, a minimum force (f_b) or binding energy (w_b) must exist between the headgroups to allow the amphiphile extraction to occur. By systematically varying the binding affinity of biotin analogues for streptavidin in SFA experiments, Leckband[21] has shown that amphiphile pull-out is favored when headgroup−headgroup binding forces exceed cohesive forces between amphiphiles in the bilayer membrane (f_m). Based on surface energy considerations, the energetic cost of withdrawing one 16-carbon dialkyl amphiphile (modeled as a cylinder) from a hydrophobic matrix into water (w_m) is $26kT$.[43] Approximating the lipid extraction potential as a square well, the theoretical force required for lipid extraction (f_m) is[21,44]

$$f_m = \frac{w_m}{l_m} = \frac{26kT}{2.0\ \text{nm}} = 6\ \mu\text{dyn} \qquad (3)$$

where l_m, the width of the potential well, is set to the length of a 16-carbon alkane. (Note that this result is independent of chain length.) Assuming that the amphiphiles are extracted individually, f_b must be ≥6 μdyn (0.06 nN) to give rise to extraction on pull-off.

The free energy of hydrogen-bond formation (w_b) in proteins is a strong function of the solvent environment. In water, w_b for amide hydrogen-bond formation is very small, about −0.5 kcal/mol or lower.[45] This result has been obtained independently by solvent transfer data as well as numerical simulations.[46,47] Honig and Yang[48] cite a value of w_b = −3.9 kcal/mol for amide hydrogen-bond

(43) Cevc, G.; Marsh, D. *Phospholipid Bilayers*: *Physical Principles and Methods*; John Wiley and Sons: New York, 1987.
(44) Bell, G. I. *Science* **1978**, *200*, 618−627.
(45) Dill, K. A. *Biochemistry* **1990**, *29*, 7133−7155.
(46) Jorgenson, W. L. *J. Am. Chem. Soc.* **1989**, *111*, 3770−3771.

formation in nonpolar solvents, based largely on solvent transfer arguments and simulation data. These values can be converted to f_b using eq 3 and assuming $l_m = 1$ Å for a hydrogen bond, yielding $f_b = 0.026$ nN for nonpolar solvents and $f_b = 0.0035$ nN for aqueous solvents. While the width of the hydrogen-bond potential well is not a precisely known quantity, the requisite force for extraction certainly meets or exceeds the value for bonding in nonpolar solvents. This has the important implication that the near-bilayer environment increases the hydrogen-bond strength to values expected for bonding in nonpolar solvents.

We emphasize that this result is based solely on the *existence* of amphiphile extraction and not a quantitative analysis of the measured pull-off force. In SFA experiments, amphiphile extraction has only been observed between strongly adherent bilayers, including measurements made between streptavidin-linked biotinylated bilayers,[21] calcium-linked carboxylic acid terminated bilayers,[41] and bilayers functionalized with complementary DNA base pairs.[25,26,49] By comparison, LB layers of the phospholipids[33,50] have pull-off forces an order of magnitude weaker, and no extraction is observed on surface separation. The occurrence of similarly strong hydrogen-bond-aided adhesions is not without precedent. Frisbie et al.[51] measured $f_b = 0.18$ nN based on AFM-derived pull-off forces between carboxylic acid terminated self-assembled monolayers (SAMs) in ethanol. Boland and Ratner[27] measured values in the range of $f_b = 0.63-1.08$ nN between nucleic-acid-functionalized SAMs in aqueous solutions. Smith et al.[52] measured strong adhesions between carboxylic and phosphonic acid SAMs and attributed strong adhesions to the formation of ionic hydrogen bonds, similar to those in the gas phase. In these measurements, functional groups are strongly bonded to the probe and surface so that extraction does not occur and a more direct measurement of f_b can be made.

A quantitative analysis of the magnitude of pull-off force identifies the efficiency of amphiphile extraction in the contact zone. The attractive part of the pull-off force $-(F/R)_{0,at}$ is related to work of adhesion (W_a) by the JKR theory:[53]

$$-\left(\frac{F}{R}\right)_{0,at} = \frac{3\pi W_a}{2} \qquad (4)$$

Assuming that the adhesion energy in our system is set by the extraction process, we calculate the maximum force per glycine amphiphile (f_e), assuming that exactly half of the amphiphiles are extracted individually (pH 5.6):

$$f_e = \frac{a_0 W_a}{l_m} = \frac{2(0.4\ \text{nm}^2)(17\ \text{mJ/m}^2)}{2.0\ \text{nm}} = 0.68\ \mu\text{dyn} \qquad (5)$$

which is much lower than $f_m = 6\ \mu$dyn calculated by eq 3. In other words, only about 12% of the amphiphiles on either surface are extracted. Because the melting transition temperature for these glycine amphiphiles is 43 °C,[54] bilayer lipids are in the gel state at room temperature and cannot quickly reorganize for most efficient headgroup bonding. Stochastic mismatches in the alignment of opposed headgroups could lead to some bonding inefficiency. It is also possible that domains of amphiphiles are extracted, not individual amphiphiles. If so, the calculated f_b would be artificially high, since multiple headgroup−headgroup bonds along the domain radius contribute to the extraction of a single amphiphile at the domain boundary. We point out that no domains were perceived by the FECO; hence, if they do exist they are smaller than 1 μm or so.

By force measurements made on functional-group variants of the glycine amphiphile, we demonstrate that amine groups need to be exposed to the interface for the strong adhesion to ensue. FTIR spectra show that amide moieties of the glycine headgroups form mutual hydrogen bonds in these LB bilayers. Because the amide group is not located at the very end of the amphiphile, it is necessary for the bilayer headgroups to rearrange or interpenetrate to bring amides from each surface together. This argument, along with the observation of a 7.5 Å decrease in bilayer thickness in adhesive contact, leads us to conclude that the mutual interpenetration of the glycine headgroups is required for the strong bonding that leads to amphiphile extraction on pull-off.

Since the glycine headgroup is a single chain as opposed to the dialkyl tailgroup, one can envision the interheadgroup spaces on each bilayer surface as "binding cavities" for glycine. Cha and co-workers[55] have shown that monolayers of oligoglycine amphiphiles with a single alkyl chain prevent the binding of soluble dipeptide groups to the monolayer. However, when dialkyl chains are used, the binding cavity formed between the glycine headgroups strongly promotes dipeptide binding.[55,56] There is also ample evidence that the binding cavity, when properly designed, can yield dramatic increases in binding energy. The Kunitake group observed million-fold increases in the binding constants of adenosine 5′-triphosphate (ATP) (or adenosine 5′-monophosphate, AMP) to Langmuir monolayers of guanidinium-functionalized amphiphiles compared to their soluble counterparts.[57,58] Large increases in binding energy for the binding cavities were also confirmed by reaction field calculations[59] and analyses of the Poisson−Boltzmann equation[60] for the interaction between soluble thymine and Langmuir monolayers of guanidinium- and diaminotriazine-functionalized amphiphiles. They found that the low dielectric constant of the amphiphile tails modulates the electrostatic potential, contributing to the stabilization of the hydrogen bonds. The amphiphile extraction we report is a measure of the force that can be transmitted by the bilayer binding cavity and agrees qualitatively with these results.

In a previous report,[32] we showed that the extraction efficiency decreases predictably with increased headgroup

(47) Torbias, D.; Sneddon, S. F., III; C. L. B. *J. Mol. Biol.* **1992**, *227*, 1244−1252.
(48) Honig, B.; Yang, A.-S. *Adv. Protein Chem.* **1995**, *46*, 27−58.
(49) Pincet, F.; Perez, E.; Bryant, G.; Lebeau, L.; Mioskowski, C. *Phys. Rev. Lett.* **1994**, *73*, 2780−2783.
(50) Marra, J. *J. Colloid Interface Sci.* **1985**, *107*, 446−458.
(51) Frisbie, C. D.; Rozsnyai, L. F.; Noy, A.; Wrighton, M. S.; Lieber, C. M. *Science* **1994**, *265*, 2071−2074.
(52) Smith, D. A.; Wallwork, M. L.; Zhang, J.; Kirkham, J.; Robinson, C.; Marsh, A.; Wong, M. *J. Phys. Chem. B* **2000**, *104*, 8862−8870.
(53) Christenson, H. K. *Langmuir* **1996**, *12*, 1404−1405.
(54) Schneider, J. W. *Force and Adhesion Measurements between Organized Layers of Protein Functional Units*; University of Minnesota: Minneapolis, MN, 1998; p 220.
(55) Cha, X.; Ariga, K.; Kunitake, T. *Bull. Chem. Soc. Jpn.* **1996**, *69*, 163−168.
(56) Cha, X.; Ariga, K.; Onda, M.; Kunitake, T. *J. Am. Chem. Soc.* **1995**, *117*, 11833−11838.
(57) Sasaki, D. Y.; Kurihara, K.; Kunitake, T. *J. Am. Chem. Soc.* **1991**, *113*, 9685−9686.
(58) Sasaki, D. Y.; Kurihara, K.; Kunitake, T. *J. Am. Chem. Soc.* **1992**, *114*, 10994−10995.
(59) Sakurai, M.; Tamagawa, H.; Inoue, Y.; Ariga, K.; Kunitake, T. *J. Phys. Chem. B* **1997**, *101*, 4810−4816.
(60) Tamagawa, H.; Sakurai, M.; Inoue, Y.; Ariga, K.; Kunitake, T. *J. Phys. Chem. B* **1997**, *101*, 4817−4825.

charging (Table 3). After subtracting double-layer repulsion from the pull-off result, the pull-off force per *uncharged* pair gave a consistent result throughout the pH range. The mechanism of this charge-induced blocking of hydrogen-bond formation can be addressed in light of these new results. Since electrostatic effects have been removed from the analysis, one possibility is that surface charging increases the surface hydration or binding of hydrated solutes. This "hydration force" could provide extra repulsion to attenuate adhesion.[61,62] However, this must be reconciled with the 7.5 Å interpenetration that is consistently observed at all pHs. Apparently, the combined effect of electrostatic and hydration forces can block interpenetration only at pH = 8.0, but at lower pH, hydration forces still attenuate the adhesion measured following interpenetration. We note that electrostatic and hydration *surface* forces may not represent a realistic mimic of the intermolecular interactions between more isolated functional groups on proteins.

To avoid complications with solute adsorption, we used low concentrations of salts with a low propensity for bilayer adsorption. Interestingly, the strong adhesion is completely extinguished by the addition of 10 mM citrate/phosphate buffer (pH 5.5), presumably due to the adsorption of buffer solutes in the binding cavity. The sensitivity of binding strength to the binding cavity size and hydration state suggests that optimization and/or modulation of the cavity properties could be exploited in the design of biosensor or microseparation systems for highly selective, tunable binding.

(61) Pashley, R. M. *J. Colloid Interface Sci.* **1981**, *83*, 531−546.
(62) Israelachvili, J. N. *Intermolecular and Surface Forces*; Academic Press: New York, 1992.

Conclusions

We have presented detailed force measurements on LB bilayers of a novel glycine-containing amphiphile using the SFA, highlighting a complex, pH-dependent competition between electrostatic, hydrogen-bonding, hydration, and hydrophobic surface forces. A remarkably strong adhesion is measured between the LB bilayers accompanied by amphiphile extraction generally observed only for strong, specific headgroup interactions between bilayers. The strength of the interaction appears to be modulated by the surface charging, extent of hydration, and size of binding cavities formed between the glycine headgroups. In this spirit, force measurements involving binding cavities may lead to a greater understanding of protein−ligand interactions and enable the rational design of responsive, selective binding surfaces for biosensors or biomaterials.

Acknowledgment. The authors acknowledge Eastman Kodak Company, the Center for Interfacial Engineering, an NSF-sponsored Engineering Research Center at the University of Minnesota, and the National Science Foundation (Grant NSF-CTS-9616797).

LA011486F